

# Swirling Effects and Occurrence in Chamfered Prismatic Tanks with Partially Loaded Condition

by Gustavo Massaki Karuka \*, *Student Member* Makoto Arai \*, *Member*  
Tomomi Yoshida\*, *Student Member* Liang Yee Cheng\*\*, *Member*  
Hideyuki Ando \*\*\*, *Member*

## Summary

An experiment was carried out to measure sloshing pressures and forces in a prismatic chamfered tank. The tank was excited laterally for regular and irregular excitation and the results were compared with numerical computations based on a Finite difference method. The tank has a Length to breadth ratio near 1, and especially in intermediate filling levels, at around the tank's 1st mode sloshing frequency, the occurrence of a rotational flow, i.e. swirling, was observed. Based on the results from both model experiment and numerical simulations, there are cases where swirling loads can be significant and therefore cannot be neglected. After checking the tank dimensions of real LNG carriers, it was noted that many actual designs have tank with the length to breadth ratio near 1 and therefore the problem can be relevant. The rotational flow characteristics and its occurrence is investigated and its pressure distribution is compared with the 1st mode sloshing, finally, considerations about the tank safety are inferred concerning the swirling problem.

## 1. Introduction

Until now, LNG carriers have been allowed to operate only under restricted filling levels. However, this might change in the near the future, as demand for partially filled levels increases. This is due to a number of reasons, such as the use of LNG as fuel, increased flexibility in LNG transportation, offshore LNG offload operations and so on.

When partially filling levels are used, there is a risk that sloshing might occur. Violent liquid motions inside the tank can generate loads that impose a danger to the tank structural integrity, and therefore it is important for the tank designer to estimate the sloshing loads magnitude and the probability of its occurrence.

A standard LNG carrier has the profile as shown in Fig. 1. After analyzing the tank dimension and arrangements of a number of LNG carriers, it was noted that tanks that use the system GTT MARKIII and NO96 have a similar cross-section, but the tank length vary depending on the design. Some of the designs have tanks to length to breadth ratio near one. Some examples can be seen in Table 1. Tanks located near the aft and forward in special, tend to be shorter in order to accommodate to the hull geometry.

When a partially filled tank has a Length to breadth ratio near 1, there is a chance that, in addition to sloshing, a rotational flow, i.e. swirling, may also occur. Most sloshing studies focus on the sloshing loads, such as in Wu<sup>1)</sup> and Kim<sup>2)</sup>, which analyzed the problem for a three-dimensional tank. Swirling studies for spherical shaped tanks can be found in Faltinsen & Timokha<sup>3)</sup> and Arai et al.<sup>4)</sup>, for example. Swirling in prismatic tanks is mentioned when tanks are excited in irregular motion in Chen<sup>5)</sup>, but in general

there is not much information available concerning the loads of swirling in membrane tanks.

In this paper, sloshing and swirling in a membrane-type LNG carrier tank is numerically simulated using a finite difference method developed by the authors Arai et al.<sup>6)</sup> for partial and full load conditions.

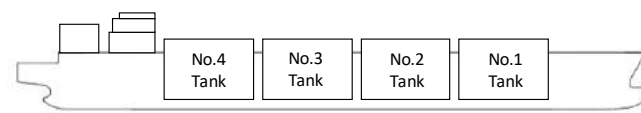


Fig. 1 General configuration of an LNG carrier.

Table 1 Tanks configuration for existing LNG carriers

Ship ID	NO.4 Tank			No.3 Tank			No.2 Tank			No.1 Tank		
	L <sub>t</sub> (m)	B <sub>t</sub> (m)	L <sub>t</sub> /B <sub>t</sub>	L <sub>t</sub> (m)	B <sub>t</sub> (m)	L <sub>t</sub> /B <sub>t</sub>	L <sub>t</sub> (m)	B <sub>t</sub> (m)	L <sub>t</sub> /B <sub>t</sub>	L <sub>t</sub> (m)	B <sub>t</sub> (m)	L <sub>t</sub> /B <sub>t</sub>
1	46.05	42.65	1.08	46.05	42.65	1.08	46.05	42.65	1.08	31.09	36.53	0.85
2	40.00	37.81	1.06	44.75	37.81	1.18	44.75	37.81	1.18	31.45	33.75	0.93
3	47.07	41.63	1.13	47.07	41.63	1.13	47.07	41.63	1.13	33.81	32.11	1.05
4	49.60	49.90	0.99	49.60	49.90	0.99	49.60	49.90	0.99	Wedge shape		
5	38.38	37.81	1.02	43.58	37.81	1.15	43.89	37.81	1.16	Wedge shape		

## 2. Numerical Method

The numerical method used in the analysis of sloshing was based on the finite difference technique. The numerical method is outlined below.

### 2.1 Governing Equations

A coordinate system  $o-xyz$  fixed to the moving tank was adopted. Assuming an incompressible and inviscid fluid, the equations governing the liquid cargo motion inside the tank are the mass continuity equation

$$\frac{\partial u}{\partial x} + \frac{\partial v}{\partial y} + \frac{\partial w}{\partial z} = 0 \quad (1)$$

and Euler's equations of motion:

\* Yokohama National University  
\*\* University of Sao Paulo  
\*\*\* Monohakobi Technology Institute

$$\begin{aligned}
\frac{\partial u}{\partial t} + u \frac{\partial u}{\partial x} + v \frac{\partial u}{\partial y} + w \frac{\partial u}{\partial z} &= -\frac{\partial p}{\rho \partial x} + \frac{f_x}{\rho} \\
\frac{\partial v}{\partial t} + u \frac{\partial v}{\partial x} + v \frac{\partial v}{\partial y} + w \frac{\partial v}{\partial z} &= -\frac{\partial p}{\rho \partial y} + \frac{f_y}{\rho} \\
\frac{\partial w}{\partial t} + u \frac{\partial w}{\partial x} + v \frac{\partial w}{\partial y} + w \frac{\partial w}{\partial z} &= -\frac{\partial p}{\rho \partial z} + \frac{f_z}{\rho}
\end{aligned} \quad (2)$$

Where

$u, v, w$ : velocity components with respect to the coordinates fixed to the tank;

$f_x, f_y$  and  $f_z$ :  $x, y$  and  $z$  components of external forces,

$p$ : pressure,

$\rho$ : density of the liquid.

The exciting motion of the tank is taken into account by the external forces  $f_x, f_y$  and  $f_z$  in the motion equations.

## 2.2 Finite Difference Approximation

To reduce the computational time and to simplify the numerical method, a staggered mesh system with constant grid spacing  $\Delta x, \Delta y$  and  $\Delta z$  in the  $x, y$  and  $z$  directions was used. The variables  $u, v$  and  $w$  were evaluated at the cell faces, while  $p$  was evaluated at the center of the grid cells. Once the initial conditions of the problem were applied, the velocities  $u, v$  and  $w$  were estimated for the next time step by using the motion equations. The variables  $u, v, w$  and  $p$  were iteratively adjusted to satisfy the continuity equation and boundary conditions. Details can be found in Arai et al.<sup>6)</sup> and Cheng et al.<sup>7)</sup>.

## 2.3 Rigid wall

Rigid boundaries are modeled by setting zero normal velocity on the wall. Free-slip with the assumption of inviscid was used.

## 2.4 Free Surface

The position of the free surface was evaluated by using a height function  $h$ , whose value was updated at every time step by applying the kinematic condition:

$$\frac{\partial h}{\partial t} + u \frac{\partial h}{\partial x} + v \frac{\partial h}{\partial y} = w \quad (3)$$

where  $h=h(t,x,y)$  is the height of the free surface measured from the tank bottom and is a function of  $t, x$  and  $y$ . The atmospheric pressure  $p_{atm}$  is set at the free surface location.

## 2.5 Impact on tank ceiling

To achieve a stable assessment of the impact pressure at the tank ceiling, a transition of the boundary condition from a free surface to a rigid wall proposed by Arai, Cheng, Kumano & Miyamoto<sup>3)</sup> and Cheng & Arai<sup>4)</sup> is considered. A detailed explanation of this condition can also be found in Cheng & Arai<sup>5)</sup>.

## 2.6 Grid size

Eight mesh sizes were tested to assess the mesh quality. In the present study, the longitudinal force  $F_x$  and transverse force  $F_y$  in the 1:40 model scale tank were chosen as the parameters to check the convergence of the results. Fig. 2 shows the maximum forces when sloshing and swirling occur. It can be observed that meshes

of the size 36x36x24 (31104 cells) or larger shows converged results. The mesh 36x36x24 was therefore chosen as the most practical in terms of computational time and result quality.

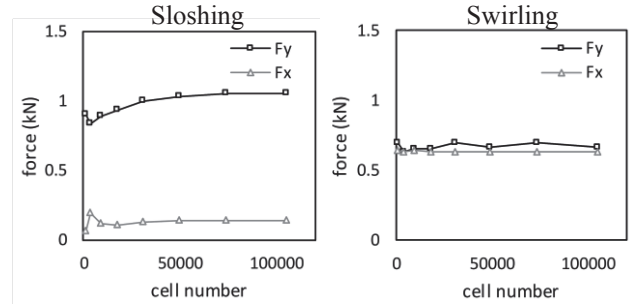


Fig. 2 Force convergence for sloshing and swirling.

## 3. Experimental setup

A series of model experiment were carried out at Monohakobi Technology Institute (MTI) Yokohama Laboratory. A 1:40 scale tank (Tank-L) was used with mounting on a moving table (Fig. 3, left). Eight pressure gauges of the type Kyowa PS-05KD were placed along the walls with an acquisition sample rate of 500 Hz. A smaller model tank of 1:68.75 scale (Tank-S) was also used to measure transverse and longitudinal forces acting on the tank (Fig. 3, right) by using a two-directional load cell. The table was excited with a regular and irregular sway motion.

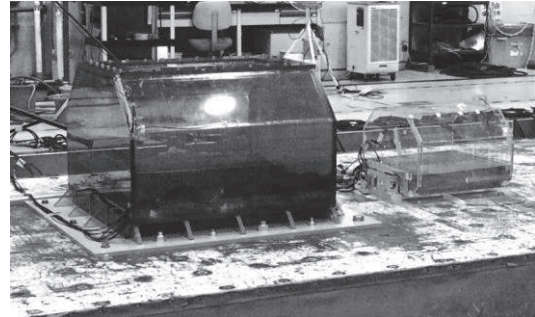


Fig. 3 Picture of tank and moving table.

### 3.1 Tank geometry and pressure gauge location

The model tank (tank-L) is a scale of a membrane tank with the Length x Breadth x Depth dimensions of 971 x 952 x 689 mm. The internal geometry of the tank and the position of the pressure gauges can be seen in Fig. 4. The tank  $L/B_t$  ratio is 1.02.

### 3.2 Experiment cases

In Table 2, the parameters used in the model test are presented. The table was excited near the natural frequency for each filling level. Then first mode of the natural frequency  $f_1$  was estimated by a simple linear theory suggested by Abrahamson<sup>8)</sup> for rectangular shaped tanks in eq. (4). A small adaptation was applied however. Instead of using the tank fixed breadth  $B_t$  in the equation, the free-surface breadth  $B_{FS}$  given a certain filling level was used when the free-surface was located at the tank chamfers.

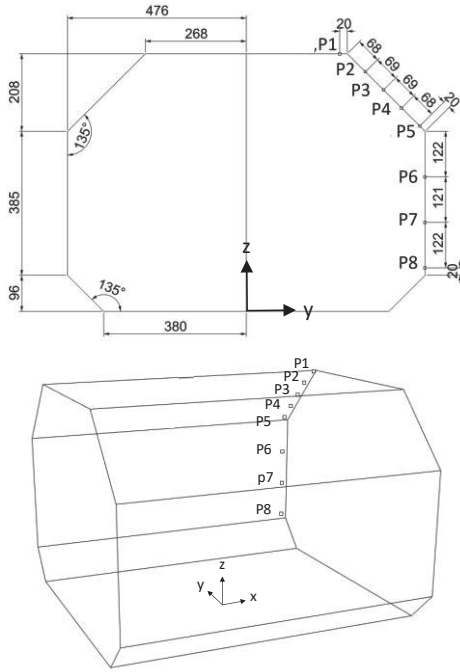


Fig. 4 Dimensions of tank model (units in mm).

$$f_1 = \frac{\sqrt{(g\pi/B_{FS}) \tanh(\pi h/B_{FS})}}{2\pi} \quad (4)$$

Table 2 test cases

Type	regular sway
Amplitude	20 mm
Frequency	$f_i, f_i+0.02, f_i-0.02$ Hz
Filling level	30%, 50%, 70%, 80%, 90%, 95%

### 4. Results

#### 4.1 Filling heights where swirling occurs

In the experiment 6 filling levels were tested, and only for 30% and 50% filling levels swirling occurred. Other filling levels were tested in the computation, and only in filling levels between 30% and 60% swirling was observed, as shown in Fig. 5. The vertical wall in the tank, which is not affected by the chamfers, goes from 14% to 70% of the tank height  $h$ . The results show that swirling develops when the free-surface height is within the vertical wall height, when the horizontal cross-section has a square shape. For heights higher than 70% or lower than 14%, the horizontal cross-section does not have a squared shape because of the chamfer, and therefore swirling does not occur.

#### 4.2 Comparison with experimental data

The numerical simulations were run with the same conditions as the experiment. The pressures were measured at the cell corresponding to the pressure gauge locations.

As shown in Fig. 6, it is possible to see the change in the pressure located in P8 with time, where sloshing developed gradually until it reaches a transition zone between sloshing and swirling. A fully developed swirling occurs after around  $t/(B_t/g)^{1/2}$

= 80. According to Fig. 6, the computational and the experimental results overlap and appear as one. Therefore, the time scale was enlarged and shown in Fig. 7. It can be observed that sloshing has 2 peaks while swirling has only one peak.

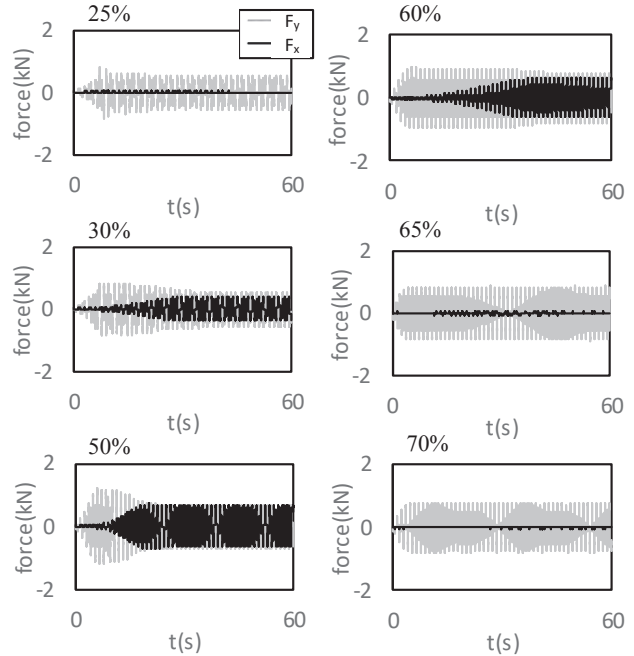


Fig. 5 Force development for different filling levels.

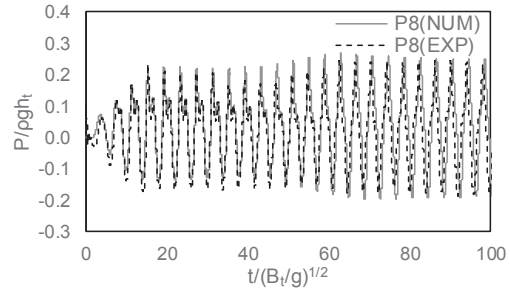


Fig. 6 50% filling level, sloshing,  $f/(g/B_t)^{1/2}=0.250$ , P8.

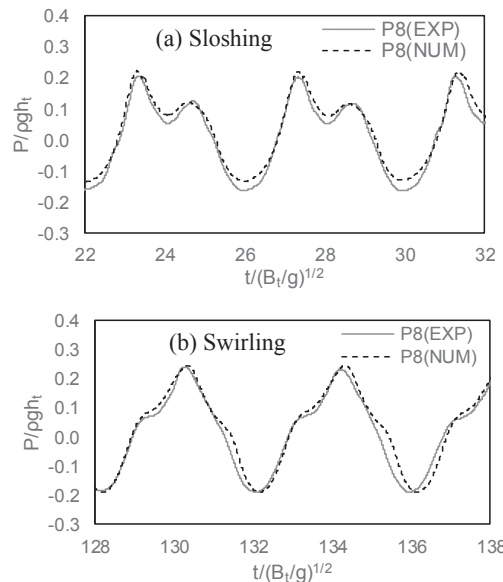


Fig. 7 50% filling level, swirling,  $f/(g/B_t)^{1/2}=0.250$ , P8.

(a) Sloshing; (b) Swirling.

Fig. 8 shows the same conditions but for the pressure gauge P5, located at the lower part of top chamfer. The pressure magnitude for swirling in this case decreases in comparison with sloshing. The impact pressure measured at P5 has a larger scatter in the experiment than numerical computation. Occasional impact pressure also occurs in swirling in the experiment.

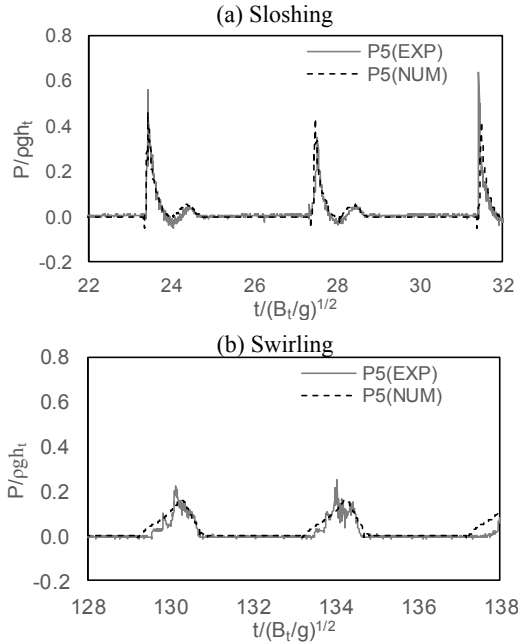


Fig. 8 50% filling level, swirling,  $f/(g/B_t)^{1/2}=0.250$ , P5. (a) Sloshing; (b) Swirling.

A 90% filling level condition was also tested. Fig. 9 show the measured pressures at P1 and P5. Both show good agreement with numerical computations but at P1, occasionally the impact pressure in the model experiment has higher peaks in comparison with the simulation. This is probably due to local effects such as a small deformation of the free surface that cannot be captured by the currently used numerical methods.

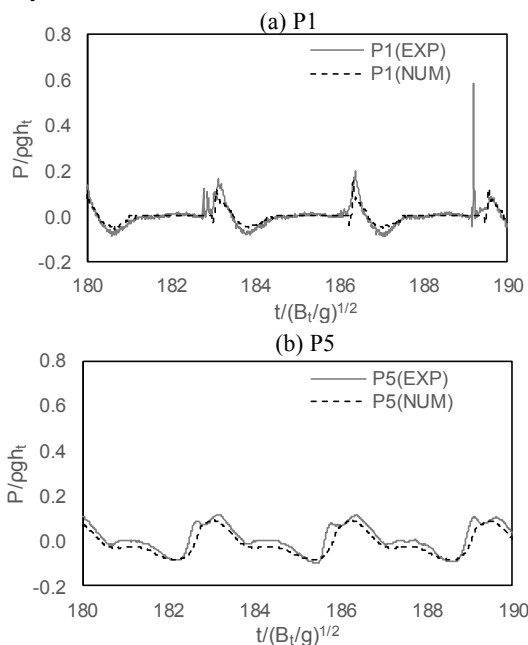


Fig. 9 90% filling level,  $f/(g/B_t)^{1/2}=0.312$ , P5. (a) P1; (b) P5

### 4.3 Considerations about swirling

When sloshing occurs, two peaks appear at the bottom pressure of the tank as shown in Fig. 10: the first peak is generated when the liquid surface reaches its maximum height, so the hydrostatic pressure at the bottom is maximum. The second peak occurs when the liquid is going lowers down, in this case there is a direction change in the flow momentum, and in consequence the dynamic pressure increases. This relation can be understood from the free surface motion shown in Fig. 11.

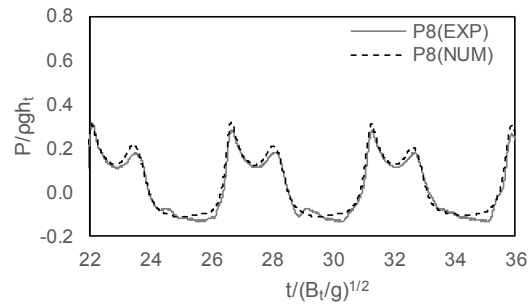


Fig. 10 30% filling level, sloshing,  $f/(g/B_t)^{1/2}=0.215$ , P8.

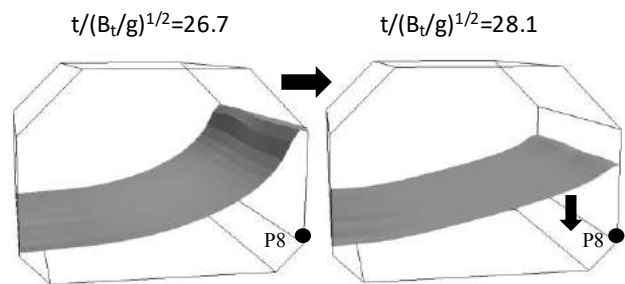


Fig. 11 Snapshots of free surface on sloshing.

The swirling flow, on the other hand, is more complex, with the liquid surface motion sometimes raising more than once in one cycle. Fig. 12 shows a swirling case in 30% filling level, where the Free-surface raises twice, resulting four peaks in the dynamic pressure.

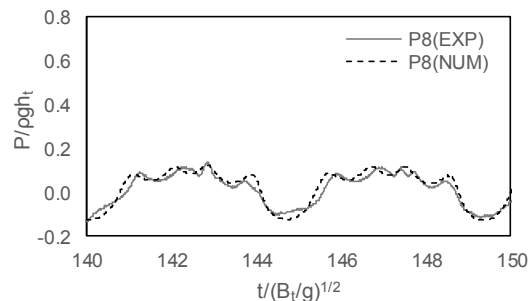


Fig. 12 30% filling level, swirling,  $f/(g/B_t)^{1/2}=0.215$ , P8.

**4.4 Influence of initial condition**

As for the rotation direction for swirling both clockwise and counter-clockwise direction appeared in the model experiment. The rotation direction seems to be sensitive to small disturbances, such as initial free-surface geometry and model tank imperfections.

In order to the rotational motion to develop, the presence of a disturbance on the longitudinal direction is necessary. This disturbance is slowly amplified until swirling develops.

In the numerical computation, because the excitation is two-dimensional and the initial free-surface is perfectly horizontal, the response is two-dimensional, in other words, pure transversal sloshing. Very small numerical errors trigger the excitation in the longitudinal direction and eventually swirling occurs.

It is easy to identify the occurrence of swirling by observing the increase of the longitudinal force  $F_x$  on the tank caused by the liquid. When the swirling is fully developed, the magnitude of the transverse force  $F_y$  and longitudinal force  $F_x$  become nearly equal, which are shown in Fig. 13(a).

By introducing a small transverse inclination intentionally to the free-surface at the initial condition, the swirling occurs earlier as shown in Fig. 13(b).

In general, the transversal forces caused by sloshing are larger than the transversal forces caused by swirling.

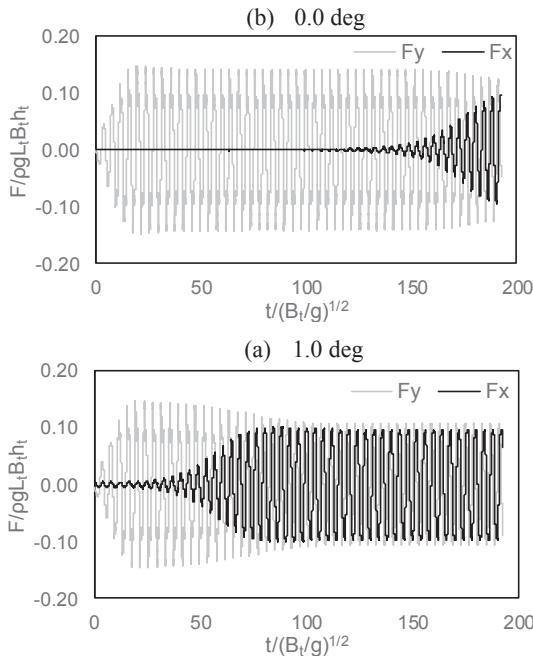


Fig. 13 Computed transversal and longitudinal forces using (a) 0deg and (b) 1deg free-surface inclination (50%filling level,  $f/(g/B_t)^{1/2}=0.250$ ,  $A_{sway}/B_t = 0.021$ ).

The larger the initial inclination angle, the faster the system converges to a stable swirling state. In Fig. 13, the time for convergence for different starting inclinations is shown. The angle 1.0 deg was chosen as the best compromise as it approaches the time for swirling convergence obtained in the experiment and at the same time it has minimum effect in the results.

The sign of the inclination also influences the direction in which swirling occurs. When the 1deg was used, the rotation developed to the clockwise direction, and when -1deg was used it developed to the counter-clockwise. Fig. 14 shows that the phase

diagram between  $F_x$  and  $F_y$  for a clockwise and counter-clockwise rotation are symmetrical to the vertical axis.

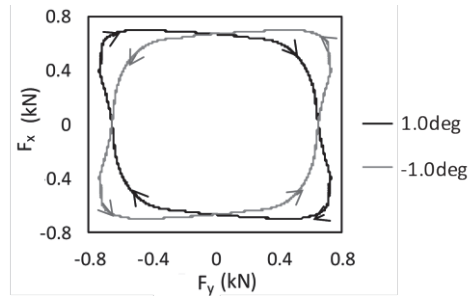


Fig. 14 Diagram phase of swirling (50%,  $L_t/B_t=1$ ,  $f_{sway}=0.84$  Hz).

**4.5 Pressure distribution in the tank**

The results below show the simulations carried out for 60 cycles. Fig. 15 shows the total pressure distribution (a) and the dynamic pressure (b).

In the experiment the pressure gauge was calibrated considering the initial pressure as zero. For the pressure gauges below the free-surface, it means that the pressure readings were subtracted by the initial hydrostatic pressure. In order to have a direct comparison between the experimental and numerical results, the same procedure was applied at the numerical results. In this study, this pressure is defined as “dynamic pressure”. As shown in Fig. 15, in the 50% filling level condition, the critical point for slosh impact pressure is near the lower part of the top chamfer. For the swirling case, in Fig. 16, the pressure in the chamfer is not as high as in the sloshing case, but a high-pressure contact occurs at the top chamfer corner when there is contact with the crest of the free-surface. The magnitude of the impact was similar to the sloshing in this case, which suggests that the impact pressure caused by swirling may not be negligible.

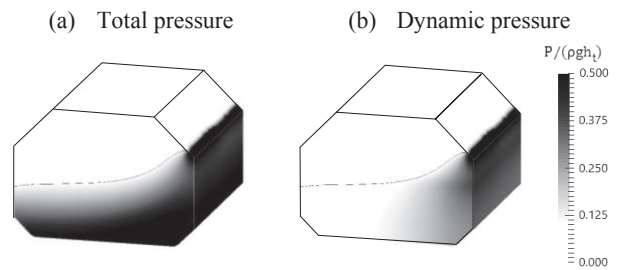


Fig. 15 Snapshot of pressure for sloshing (50%filling level,  $f/(g/B_t)^{1/2}=0.250$ ,  $A_{sway}/B_t = 0.021$ ).

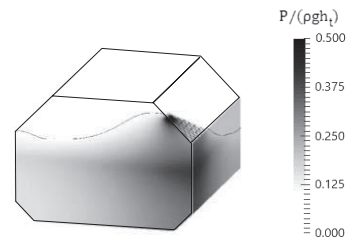


Fig. 16 Snapshot of dynamic pressure for swirling (50%filling level,  $f/(g/B_t)^{1/2}=0.250$ ,  $A_{sway}/B_t = 0.021$ ).

Fig. 17 shows the maximum dynamic pressure distribution for the whole simulation time for 30%, 50%, 90% and 95% filling levels. For 30% and 50% it can be observed that the lower part of the top chamfer suffers the highest pressure. For 50%, in the maximum pressure distribution there is a slight increase in pressure at the top chamfer corner due to swirling. For 90% filling level, not a significant dynamic pressure is detected. For 95%, high pressure appears at the ceiling edge, especially near corners. This suggests that tanks with filling levels near the full load condition may also be susceptible to high impact pressure.

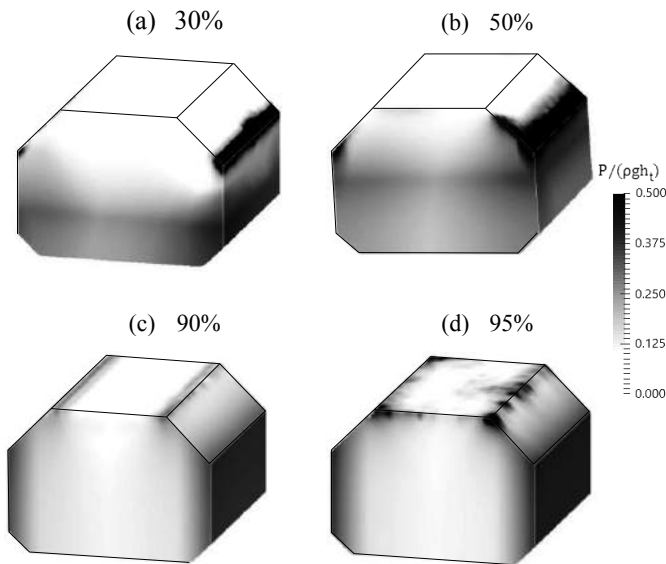


Fig. 17 Max dynamic pressure, (sway amplitude)/ $B_t = 0.021$ ;  
 (a) 30% filling level,  $f/(g/B_t)^{1/2} = 0.215$ ;  
 (b) 50% filling level,  $f/(g/B_t)^{1/2} = 0.250$ ;  
 (c) 90% filling level,  $f/(g/B_t)^{1/2} = 0.312$ ;  
 (d) 95% filling level,  $f/(g/B_t)^{1/2} = 0.333$ .

4.6 Swirling for different  $L/B_t$  ratios

A 50% filled tank excited in different frequencies with  $A_{sway}/B_t = 0.021$  is shown in Fig. 18. Near the natural frequency ( $f = 0.804$  Hz), swirling can be identified with the  $F_x/F_y$  ratio near 1. Another way of identifying swirling occurrence is by checking the parametric curve with  $F_x$  and  $F_y$ . In Fig. 19, it is possible to see that in (b) and (c), when swirling occurs, the phase diagram has the shape between a circle and a square. In (a) and (d), where pure sloshing occurs, the phase diagram has the shape of a straight line, which means that only transverse force is generated.

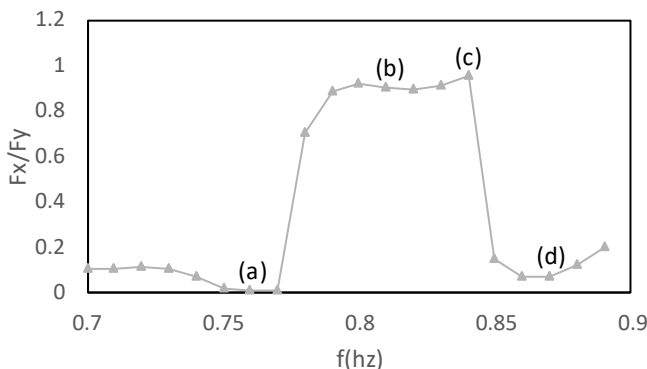


Fig. 18 Example of  $F_x/F_y$  (50%,  $L/B_t = 1.0$ ).

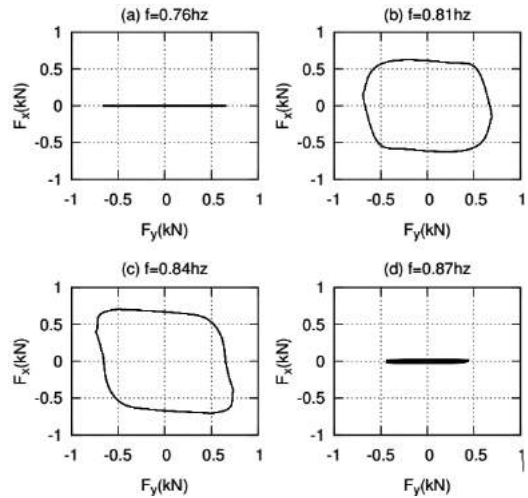


Fig. 19 Parametric curve of  $F_x$  and  $F_y$ .

In Fig. 20, the case from in Fig. 18 is further detailed. A 2D computation was carried out to analyze the case where pure sloshing occurs. In this case the transverse force  $F_y$  reach its peak near  $f_{ly}$ . In the 3D case, swirling develops near  $f_{ly}$ , and the maximum transverse force is lower than in the sloshing case, with swirling occurring for a range of frequencies slightly higher than the  $f_{ly}$ .

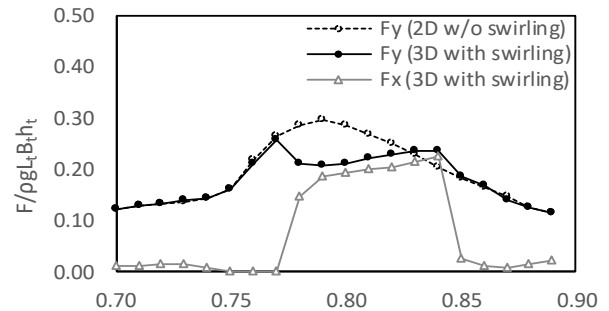


Fig. 20  $F_x$  and  $F_y$  for 2D and 3D simulations

In order to understand the swirling for tanks with different  $L/B_t$  ratio, the tank model used in the study was slightly modified and tested. The tanks were excited with a regular sway excitation,  $A_{sway}/B_t = 0.021$ . Fig. 21 shows the  $F_x/F_y$  ratio for tanks with different  $L/B_t$  ratio for four conditions: 30%, 40%, 50% and 60% filling levels. It can be clearly seen that the swirling occurs with high intensity when  $L/B_t$  ratio is near 1. For all cases swirling occurs, although in different intensities, in a range that goes approximately from  $L/B_t$  of 0.9 to 1.10.

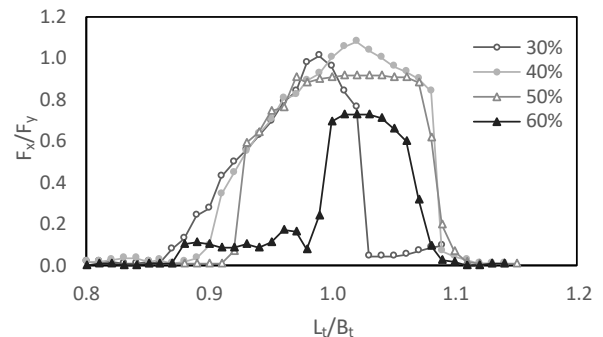


Fig. 21  $F_x/F_y$  for different filling levels.

Three tanks with  $L_t/B_t$  of 0.94, 1.00 and 1.06 were tested for different lateral excitations. The transverse natural frequency  $f_{ly}$  and longitudinal natural frequency  $f_{lx}$  is shown in Table 3. In Fig. 22, it can be observed that when  $L_t/B_t$  is 1.0, the sway occurrence range is around  $f_{ly}$ , which is equal to  $f_{lx}$ . For  $L_t/B_t$  0.94 and 1.06 the swirling range occurs is displaced towards a frequency between  $f_{ly}$  and  $f_{lx}$ . Since the prismatic tank is a 3-dimensional, the tank can be excited in two directions. Swirling happens when the transverse and longitudinal are excited simultaneously. For this reason, swirling happens in frequency range centered between  $f_{ly}$  and  $f_{lx}$ .

Table 3 Natural frequencies for tanks with different length to breadth ratio

$L_t/B_t$	$L_t$ (m)	$B_t$ (m)	$f_{lx}$ (Hz)	$f_{ly}$ (Hz)
0.94	0.913	0.971	0.842	0.805
1.00	0.971	0.971	0.805	0.805
1.06	1.029	0.971	0.770	0.805

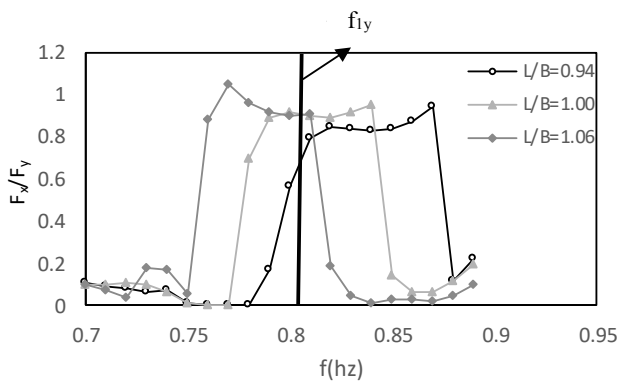


Fig. 22  $F_x/F_y$  for different frequencies.

#### 4.7 Responses by irregular excitation

In order to study the sloshing response in irregular seaways, the model tank (Tank-S) was excited on a moving table with irregular sway motions. The time histories of the tank's sway motion were prepared using the typical wave spectrum data and the ship's sway motion RAO (Response Amplitude Operator). The measured and computed time histories of  $F_x$  and  $F_y$  are compared in Fig. 23. The force and time scales in Fig. 23 are converted from the model scale to the actual ship scale using Froude's law. Although, the same time history of the tank motion was used in the model experiment and the numerical simulation, the measured and computed force histories did not perfectly match each other. One possible reason for this is the difference in the rotating direction, i.e., clockwise or anti-clockwise, of the liquid motion in the tank. As observed in the model experiments with regular excitation, a small disturbance in the flow can trigger the swirling and determine the direction of the rotating motion. Incidentally, either clockwise or anti-clockwise motion may start. The swirling motion couples with the sloshing motion, and the accumulated liquid motion response changes the liquid motion time history afterward. Therefore, it was very difficult to numerically simulate the time histories of the force under irregular excitation. However, in some parts of the force time histories, very similar patterns were reproduced by our numerical computation. One example of such a case is shown in Fig. 24 and

Fig. 25. A part of the time histories presented in Fig. 23 is shown with an enlarged time scale in Fig. 24 and Fig. 25. As shown in this figure, the computed  $F_y$ , the lateral force, agrees well with the measured one in this period (Fig. 24). On the other hand, the computed  $F_x$ , the longitudinal force, did not match the measured one (Fig. 25 (a)). As shown in Fig. 25 (b), however, if we reverse the sign of the force it agrees quite well with the measured data. This means that the rotating direction of the numerical simulation Fig. 25 (a) was the opposite to that of the measured one.

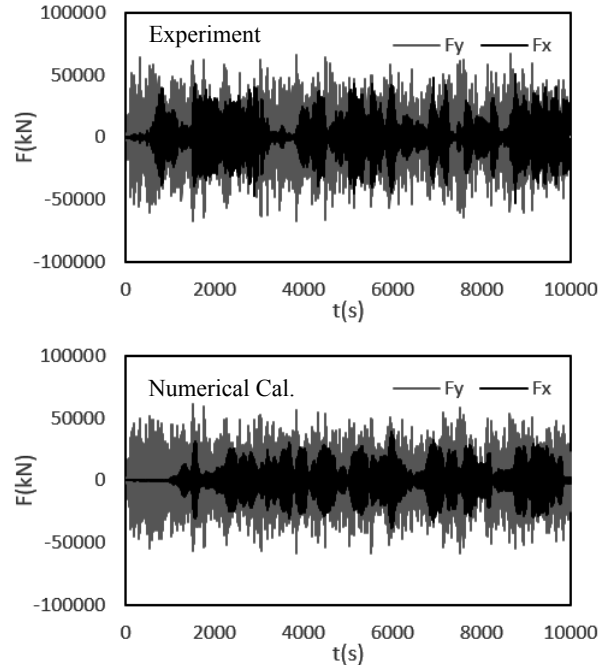


Fig. 23 Comparison of measured and computed force histories (irregular sway motion,  $H_{1/3}=5.89$  m,  $T_{mean}=9.55$  s on actual ship scale).

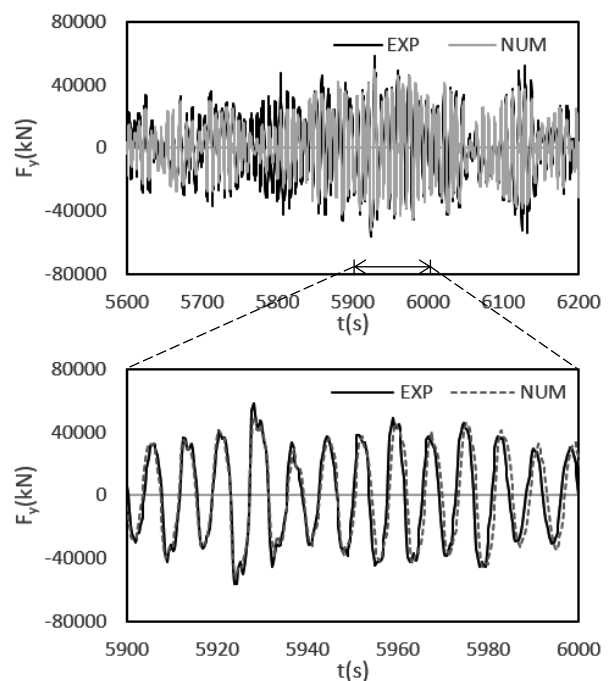


Fig. 24 Comparison of measured and computed  $F_y$  histories (part of Fig.24 is enlarged in time, irregular sway motion,  $H_{1/3}=5.89$  m,  $T_{mean}=9.55$  s on actual ship scale).

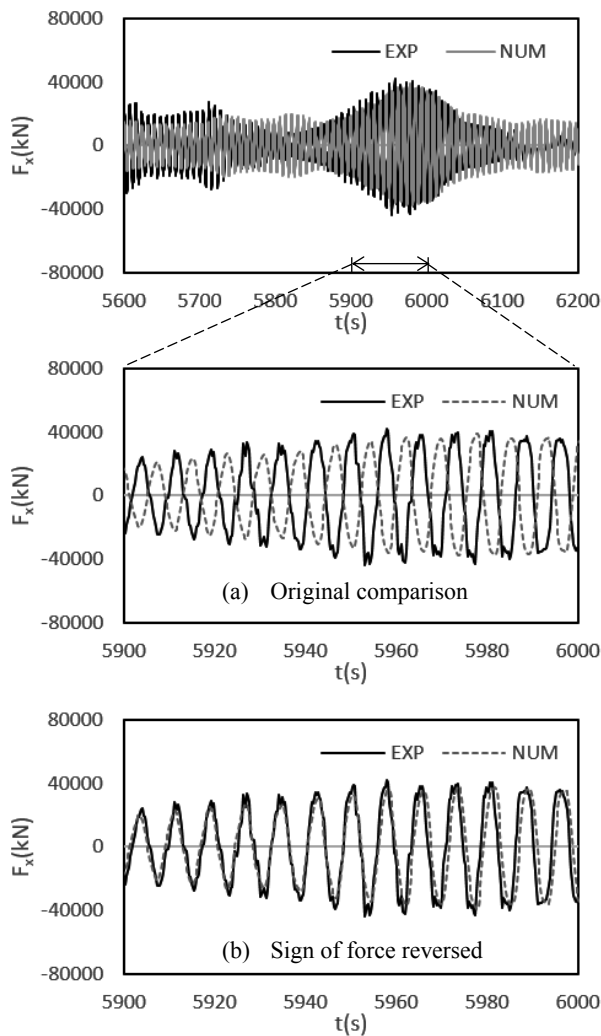


Fig. 25 Comparison of measured and computed  $F_x$  histories (part of Fig.25 is enlarged in time, irregular sway motion,  $H_{1/3}=5.89$  m,  $T_{mean}=9.55$  s on actual ship scale).

## 5. Conclusions

In this study, a series of simulations for different filling levels were carried out and compared with experimental data. The general fluid motion and dynamic pressures obtained by the numerical simulation agreed well with experimental data, confirming the suitability of the numerical tool to represent the phenomenon. However very localized impact pressures are sometimes not well captured in the simulation. This may be mainly due to local effects such as jet and spray formation, surface tension, the interaction between air and liquid and air cushioning effects.

For filling levels between 30% and 60%, swirling may occur if the length to breadth ratio of the tank is between 0.90 and 1.10. The frequency in which the phenomena is most intense is located between the transverse and longitudinal natural frequencies of the tank.

A 3D representation of the maximum dynamic pressure was shown. Although the swirling loads were in general smaller than the sloshing loads. In some cases, swirling had a significant impact on areas that differ from the sloshing impacts. Some LNG carriers

were found to have a tank ratio near 1, and for these designs, swirling should be considered.

It is possible to see that although high filling levels like 95% are accepted as safe, high impact pressure can still occur at the tank ceiling, and this should be noted by the designers.

In the irregular excitation test, some differences between the experimental and the numerical data were found. One of the reasons is due to the fact that the rotation direction of the fluid has a random nature that is not easily predicted in the computation.

## 6. Acknowledgments

Part of this research was carried out as ClassNK's Joint R&D with Industries and Academic Partners project. The authors would like to express their gratitude to ClassNK for their support.

## 7. References

- 1) Wu G.X., Ma Q.W, Taylor R.E.: Numerical simulation of sloshing waves in a 3D tank based on a finite element method. Applied Ocean Research; Vol.20, Issue 6, pp.337-355, 1998
- 2) Kim Y., Shin Y.S., Lee K.H.: Numerical study on slosh-induced impact pressures on 3-D prismatic tanks, Applied Ocean Research. Vol 26, pp. 213-226, 2004
- 3) Faltisen, O.M., Timokha A.: Nonlinear sloshing in a spherical tank, Conference Proceedings, OMAE, 2013
- 4) Arai M., Cheng L.Y., Wang X., Okamoto N., Hata R., Gustavo M.K.: Sloshing and swirling behavior of liquid in a spherical LNG tank, Proceedings of International Symposium on Ships and Other Floating Structures PRADS, 2016
- 5) Chen B.F., Wu C.H.: Effects of excitation angle and coupled heave-surge-sway motion on fluid sloshing in a three-dimensional tank, Journal of Marine Science and Technology, Vol. 16, Issue 1, pp. 22-50, 2011
- 6) Arai M., Cheng, L. Y., Kumano, A., Miyamoto, T., A.: Technique for Stable Numerical Computation of Hydrodynamic Impact Pressure in Sloshing Simulation, Journal of the Society of Naval Architects, Japan, Vol. 191, pp. 299-307, 2002
- 7) Cheng, L. Y., Arai, M.: A 3D Numerical Method for Assessment of Impact Loads Due to Sloshing in Liquid Cargo Tanks, Proceedings of the Fifteenth International Offshore and Polar Engineering Conference, pp. 214-221, 2005
- 8) Abramson H. M., Bass R. L., Faltinsen O.M., Olsen H.A.: Liquid Slosh in LNG Carriers, 10th Naval Hydrodynamics Symposium, pp.21-38, 1974